Spectral induced polarization monitoring of toluene biodegradation by Rhodococcus wratislaviensis in controlled laboratory conditions

Urie L Zohoré, Pauline Kessouri, Jacques Deparis, Marc Crampon, Roger Guérin, Damien Jougnot

Geophysical Journal International

Geophys. J. Int. (2026) **244,** 1–13
Advance Access publication 2025 November 29
Research Paper

https://doi.org/10.1093/gji/ggaf486

Spectral induced polarization monitoring of toluene biodegradation by *Rhodococcus wratislaviensis* in controlled laboratory conditions

Urie L. Zohoré [1,2] Pauline Kessouri,[2] Jacques Deparis,[2] Marc Crampon,[2] Roger Guérin[1] and Damien Jougnot [1]

[1] *Sorbonne Université, CNRS, EPHE, UMR* 7619 *METIS,* 75005 *Paris, France. Email: zohore.urie@gmail.com*
[2] *BRGM, Service Géologique National,* 45060 *Orléans, France*

Accepted 2025 November 24. Received 2025 November 19; in original form 2025 January 23

SUMMARY

The global prevalence of organic pollutants presents a significant environmental challenge, necessitating sustainable remediation strategies. *In situ* biodegradation emerges as a cost-effective and eco-friendly solution. However, the real-time monitoring of *in situ* bacterial activities, particularly biodegradation processes, remains a challenge due to the limitations of traditional intrusive methods, including issues of representativeness, reproducibility and high-associated costs. Spectral induced polarization (SIP) has shown sensitivity to surface changes in subsurface environments, especially for biogeochemical reactivity monitoring including those associated with biodegradation. Despite this potential, advances have to be made to quantitatively link SIP parameters to *in situ* biodegradation processes. This study addresses this gap by conducting controlled biogeophysical experiments on a sand-packed column undergoing biodegradation facilitated by *Rhodococcus wratislaviensis* IFP 2006. SIP measurements were paired with bacterial growth kinetics to develop a quantitative model estimating bacterial growth. The results demonstrate that SIP, coupled with routine laboratory measurements, can effectively and quantitatively assess bacterial growth and the biodegradation of organic pollutants. These findings highlight the potential of SIP as a non-intrusive and reliable method for monitoring biodegradation in contaminated subsurface environments.

Key words: Electrical properties; Permeability and porosity.

1 INTRODUCTION

Environmental pollution from organic compounds is a global issue. Petroleum hydrocarbon leaks and accidental spills are frequent occurrences. These incidents, stemming from anthropogenic activities, can arise at any stage of the fuel production chain, including extraction, refining, transportation and storage (M. Saeedi *et al.* 2024; M. Kamranifar *et al.* 2025). Once released into the environment, certain fractions of petroleum hydrocarbons exhibit high-toxicity potential, posing significant risks to ecosystems (e.g. Chikere *et al.* 2011), water resources (e.g. Truskewycz *et al.* 2019) and human health (Ball & Truskewycz 2013). The challenge of a growing global population necessitates the implementation of efficient remediation techniques to mitigate adverse effects on health and the environment.

Bioremediation holds significant potential to effectively restore polluted environments by harnessing the degradation capabilities of microorganisms (Warhurst & Fewson 1994; Martínková *et al.* 2009; Kuyukina & Ivshina 2019). Enhanced and/or natural bioremediation has been recognized as a non-invasive and cost-efficient approach for remediating soil and aquifers contaminated with BTEX (benzene, toluene, ethylbenzene, xylene) hydrocarbons (e.g. van der Geize & Dijkhuizen 2004a; Mellage *et al.* 2015). *In situ* monitoring of biodegradation can be challenging due to the direct inaccessibility to pollution (De Souza *et al.* 2024; Kuppan *et al.* 2024). However, geoelectrical methods and spectral induced polarization (SIP) in particular have shown promise for indirectly monitoring subsurface microbial activity by detecting geoelectrical signatures associated with biogeochemical processes (Kessouri *et al.* 2019). Indeed, the sensitivity of SIP to bacterial activities and growth has been successfully demonstrated through numerous laboratory experiments (Abdel Aal *et al.* 2004, 2006; Ntarlagiannis *et al.* 2005; Davis *et al.* 2006; Mewafy *et al.* 2013; Zhang *et al.* 2014; Noel *et al.* 2016; Rosier *et al.* 2019; Zhang & Furman 2023; Saneiyan *et al.* 2024). Moreover, to better describe changes occurring in the chemical properties of geological media, geoelectrical tools are used in conjunction with geochemical measurements: pH, redox potential, fluid electrical conductivity and dissolved oxygen content (Noel *et al.* 2016; Joo *et al.* 2021; Rembert *et al.* 2025).

These past years, there has been an effort towards developing a quantitative approach to mechanistically link SIP measurements to bacterial growth (Revil *et al.* 2012; Zhang *et al.* 2014; Mellage *et al.*

2015, 2018; Joo *et al.* 2021; Song *et al.* 2022, 2024). However, all of these studies used glucose as the main carbon source or lactate, which is a by-product of glucose metabolism. Glucose is commonly used as the primary substrate for cultivating microorganisms under controlled conditions (Carreón-Rodríguez *et al.* 2023); however, it is not representative of substrates found in hydrocarbon contaminated environments.

This paper investigates the use of the SIP method to monitor in real-time the *in situ* biodegradation processes and quantitatively link them with the measured SIP parameters. We investigate the degradation of toluene by *Rhodococcus wratislaviensis* IFP 2006 (*R. wratislaviensis*), growing on a toluene substrate. This substrate allows us to monitor biodegradation in conditions closer to the field conditions at a hydrocarbon-contaminated site. We present the complete biodegradation process, starting with bacterial colonization of an abiotic environment and demonstrating their growth using an organic pollutant as the sole carbon source. Our objectives are twofold: (1) to assess the temporal evolution of SIP signals in a sand-packed column undergoing biodegradation by *R. wratislaviensis,* and (2) to apply a quantitative, SIP-based model proposed by Revil *et al.* (2012) to estimate bacterial growth and decay kinetics. After some theoretical reminders and practical descriptions on the geophysical and biogeochemical methods used in this study, we introduce the geochemical monitoring results. We then present the SIP monitoring results and compare them with the biological tracers. We finish by discussing the biodegradation dynamics of toluene during our experimentations and the predicted bacterial evolution using Revil *et al.* (2012) model.

2 THEORETICAL BACKGROUND

2.1 Bacterial evolution

The growth of a microbial population after colonizing a new environment follows a well-known cycle, consisting of the lag, exponential, stationary and decline phases (Buchanan 1918; Zwietering *et al.* 1990; Konhauser 2007; Madigan *et al.* 2010; Nelson & Cox 2013). The lag phase corresponds to the time when bacteria adapt to their new environment, sometimes requiring the synthesis of new enzymes. During the exponential phase, once acclimated, cells begin to reproduce rapidly. This phase is characterized by a significant increase in biomass. However, exponential growth cannot continue indefinitely. This is due to nutrient depletion, the accumulation of toxic waste products and changes in the local culture environment that can negatively affect the cells. At the stationary phase, there is no net increase or decrease in the total number of cells. Some bacteria continue to grow actively while others die. As conditions continue to deteriorate for the population as a whole, a large number of cells die, leading to the decline phase.

In liquid or solid media, bacteria can be present in two phenotypic phases: either as planktonic (free floating) or immobilized in a surface attached biofilm (Moore-Ott *et al.* 2022). Biofilms are aggregations of bacterial cells attached to a surface. Their formation is a multistep process beginning with the initial attachment of individual cells or small clusters. In this first step, planktonic cells are transported to the surface, where initial, reversible adhesion is facilitated by physical forces such as van der Waals interactions, electrostatic forces and hydrophobic interactions (Palmer *et al.* 2007). The transition to a mature biofilm occurs as these attached cells proliferate and secrete significant extracellular polymeric matrix (Madigan *et al.* 2010). This matrix consists mainly of polysaccharides and can also contain proteins and nucleic acids (Madigan *et al.* 2010). It is considered that bacteria prefer growth in biofilm for four main reasons: microbial self-protection, maintenance in a favourable environment, close association lifestyle for communication, gene transfers and natural growth mode (Madigan *et al.* 2010; Mirghani *et al.* 2022; Moore-Ott *et al.* 2022).

Once mature, environmental stresses such as nutrient limitation or oxygen depletion can trigger a dispersion phase, during which cells are released from the biofilm into the surrounding liquid (Petrova & Sauer 2016; Berne *et al.* 2018). These dispersed cells can subsequently attach to new surfaces and initiate further colonization, completing the biofilm life cycle.

2.2 SIP method and parameter definitions

The SIP method extends the conventional electrical conductivity approach, which measures a material's response at a single frequency or under direct current, by measuring the complex conductivity over a wide frequency range (from the mHz to the kHz). This technique involves injecting a sinusoidal electrical current into a rock sample and measuring the resulting electrical potential difference. SIP parameters are determined from measuring the impedance magnitude $|Z|$ (Ω) and the phase shift φ (rad) between the voltage measured and the injected current. In the SIP method, the measured electrical response is expressed in terms of complex conductivity, which can be described by the following relations:

$$\sigma^* = \frac{1}{\rho^*} = \sigma' + i\sigma'', \tag{1}$$

where $i = (-1)^{1/2}$ is the imaginary unit and the real σ' (S m^{-1}) and imaginary σ'' (S m^{-1}) components of complex conductivity are frequency-dependent and calculated from the measured parameters as follows

$$\sigma' = \cos(\varphi)/(k|Z|) = |\sigma|\cos(\varphi), \tag{2}$$

$$\sigma'' = \sin(\varphi)/(k|Z|) = |\sigma|\sin(\varphi), \tag{3}$$

where k (m) refers to the geometrical factor linked to the electrode configuration and cross-sectional area of the measured sample. These parameters can be linked to physical, chemical and biological properties of the medium through petrophysical relationships (e.g. Kemna *et al.* 2012). According to the formulation of Slater & Lesmes (2002), the complex conductivity for a saturated medium can be expressed as

$$\sigma^* = \left[\sigma_w \phi^m + \sigma'_{surf}\right] + i\sigma''_{surf}, \tag{4}$$

where σ_w (S m^{-1}) is the conductivity of the electrolyte saturating the pores, ϕ is the porosity (-) and m is the cementation factor (-) from Archie (1942). The real component of the complex conductivity represents ohmic conduction currents, including the conductivity of the pore-saturating fluid and a contribution from interfacial conductivity σ'_{surf}. The imaginary component of the complex conductivity σ''_{surf} represents the polarization effects within the samples that include, below 10 kHz, interfacial polarization mechanisms: e.g. the Maxwell–Wagner effect, the electrical double layer polarization and the membrane polarization. In the absence of metallic minerals and presence of bacteria, both σ'_{surf} (S m^{-1}) and σ''_{surf} (S m^{-1}) result from the formation of an electrical double layer (EDL) at the grain–fluid interface (Revil & Glover 1998) and bacteria–fluid interface (van der Wal *et al.* 1997).

2.3 SIP signature of bacterial growth

The polarization mechanism of bacteria is due to their negatively charged membrane. It is thought that the low-frequency (<100 Hz) polarization mechanism of bacterial cells and clay particles is similar and relates to the formation of an EDL around their surfaces (van der Wal *et al.* 1997; Grosse 2002; Revil *et al.* 2012).

Based on this assumption, Revil *et al.* (2012) proposed a quantitative model to determine bacterial growth kinetics from knowing the imaginary conductivity:

$$\sigma_B^{''}(t) = {}'(t_0)\exp\left\{Aexp\left[-\exp\left[\frac{\mu_m e}{A}(\tau - t) + 1\right]\right]\right\}, \quad (5)$$

$$\sigma''(t) = \sigma_B^{M''}\exp[-k_d(t - t_0)] + \sigma_S^{''}, \quad (6)$$

where $'(t_0)$ (S m^{-1}) denotes the imaginary conductivity right after the inoculation phase and t_0 is the time (d) characterizing the beginning of this phase, $\sigma_B^{M''}$ (S m^{-1}) denotes the imaginary conductivity at the beginning of the decay curve,

$$A = ln\left(\sigma_B^{M''}/'\right), \quad (7)$$

μ_m (d^{-1}) is the maximum specific growth rate coefficient, $e = \exp(1)$, τ (d) represents the lag time prior to bacterial rapid growth, $\sigma^{''}(t)$ is the total imaginary conductivity of the sand column, k_d (d^{-1}) is the first-order rate coefficient for endogenous respiration, and $\sigma_S^{''}$ (S m^{-1}) the imaginary conductivity of the sandy background.

The authors adapted two microbial growth models to predict the imaginary conductivity response during the bacterial growth and decay stages. The first of the two models is the Gompertz function reparametrized by Zwietering *et al.* (1990) which predicts bacterial growth in the case where the substrate is a non-limiting factor,

$$C_B(t) = C_B^0(t_0)\exp\left\{A'\exp\left[-\exp\left[\frac{\mu_m e}{A'}(\tau - t) + 1\right]\right]\right\}, \quad (8)$$

and the Monod equation which relates bacterial concentration to a limiting nutrient (Monod 1949):

$$C(t) = C_B^M \exp\left[-k_d(t - t_0)\right], \quad (9)$$

where C_B (number of cells per mL) is the bacteria cell concentration, C_B^0 (number of cells per mL) denotes initial bacterial cell concentration, C_B^M (number of cells per mL) represents the maximal bacterial cell concentration, and

$$A' = \ln\left(C_B^M/C_B^0\right). \quad (10)$$

The principle behind these equations is quite straightforward. Based on the bacterial evolution described in Section 2.1, general bacterial growth can be modelled considering both the growth and mortality rates. Bacterial growth exhibits a phase during which the specific growth rate starts at zero (lag phase) and then accelerates until reaching a maximum value (μ_m at the end of the exponential phase) over a certain period. Additionally, growth curves show a final phase during which the rate gradually declines to zero, leading to an asymptote (A during the stationary phase). Finally, as conditions deteriorate, the bacteria die following an exponential decline characterized by a decay rate k_d.

3 MATERIALS AND METHODS

3.1 Sample characterization and preparation

The host porous medium used in this experiment was a silicate sand composed of 99 per cent quartz (BB 0.7/1.3, Sibelco, France). The sand grain radius distribution ranged from 0.5 to 1.6 mm, with a median value of 1.01 mm. Additionally, it served as a stable base material resistant to alteration up to a pH of 9.75 (Dove & Elston 1992), making it particularly useful for chemical analysis interpretation. The sand used in this study underwent a series of sterilization steps prior to the experiments.

It has been treated with acidic (HCl) and basic (NaOH) solutions to remove its $CaCO_3$, organic matter and metals content following an adapted version of Ben Moshe *et al.* (2021) treatment procedure. This procedure has been adopted to reduce the amount of ions adsorbed on the sand particle surfaces, thereby minimizing any influence (other than ions from this study's electrolytes) on the SIP response. The second treatment aimed at sterilizing the sand. Indeed, it was placed in an oven at 100 °C for 36 hr to dry. Subsequently, it was autoclaved three times for 1 hr at 120 °C over 3 d. Each autoclaving phase aimed at eliminating the active cells but not necessarily the spores. These can become active cells at 24-hr intervals (Noel *et al.* 2016). Thus, repeating the autoclave procedure allowed for an important reduction in pre-existing bacterial strains.

Table 1. Chemical composition of growth medium.

Compound	Concentration (g L^{-1})
Vitamins	0.44
Oligo elements	5.9
NH_4NO_3	1.5
$MgSO_4$	0.5
$CaCl_2$	0.04
KH_2PO_4	140
K_2HPO_4	170

3.2 Bacterial culture preparation

R. wratislaviensis is an aerobic, rod-shaped and gram-positive bacterium. Its optimal growth conditions include a temperature in the range of 20–30 °C and a neutral pH (Kuyukina & Ivshina 2019). The genus *Rhodococcus* has been extensively studied in literature and is known for its ability to degrade a broad range of organic compounds such as petroleum hydrocarbons, chlorinated, nitrogenated and other complex organics (Auffret *et al.* 2009; Noel *et al.* 2016; Kuyukina & Ivshina 2019). Its occurrence settings include soils, waters and air. The biodegradation potential of this genus relates to its diverse catabolic and enzymatic capabilities (van der Geize & Dijkhuizen 2004; Martínková *et al.* 2009). In this study, the strain of *R. wratislaviensis* has been used to biodegrade toluene, a major component of diesel and oil contaminated sites.

The growth medium was made up with solutions of vitamins, oligo elements, mineral salts (NH_4NO_3: 1.5 g L^{-1}; $MgSO_4$: 0.5 g L^{-1}; $CaCl_2$: 0.04 g L^{-1}; and potassium phosphate KH_2PO_4/K_2HPO_4 buffer solution) and toluene. The chemical composition of the growth medium is summarized in Table 1.

The bacterial solution used to inoculate the sand column has been prepared as follows. The strain was precultured for 3 d (towards the end of the exponential phase) to obtain a total volume of 6 L of bacterial solution. The centrifuged cells were placed into 2 L of a fresh growth medium containing 25 mg L^{-1} dissolved toluene. Then, this volume was centrifuged at 4500 rpm (rotation per minute) for 10 min to extract bacterial cells without damaging their membranes (Peterson *et al.* 2012). The centrifugation process was aimed at achieving a high-initial bacterial concentration. This highly concentrated bacterial solution was used as the inoculum for the sand packed column. The initial bacterial concentration was estimated at 2×10^{10} bacteria mL^{-1} from microscopic direct cell count on

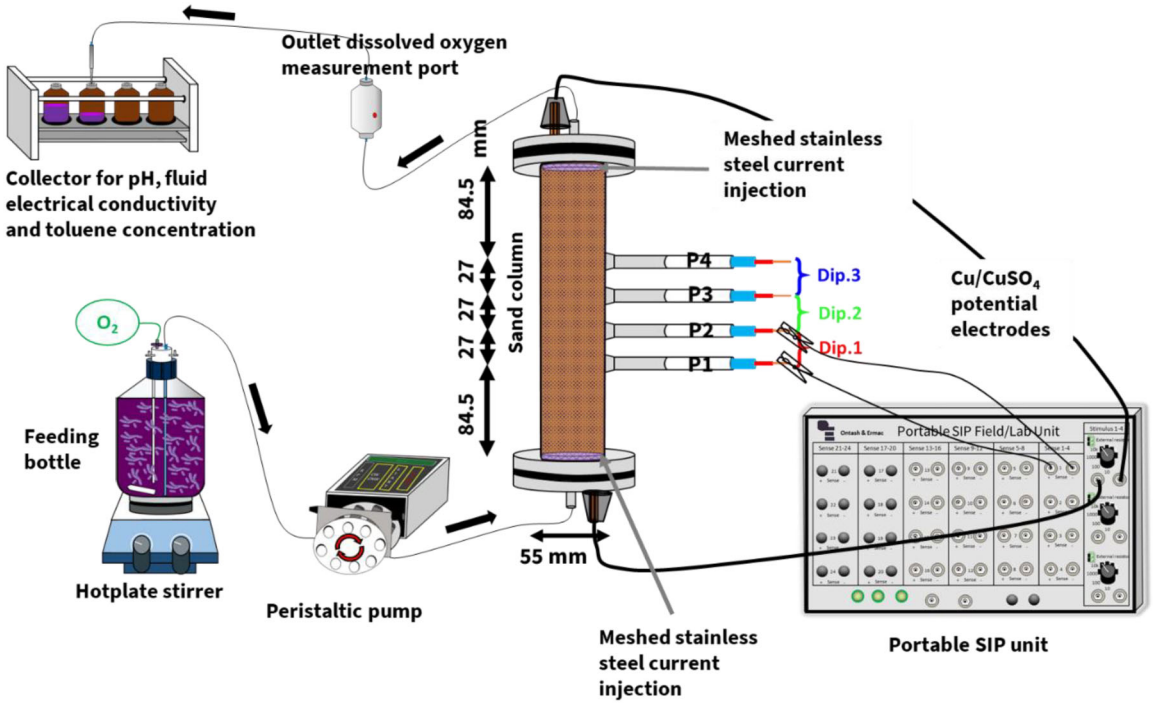

Figure 1. Schematic representation of the experimental setup: The porous column system is fed by a peristaltic pump providing a fixed flow rate. The effluent at the outlet is sampled using a fraction collector. SIP measurements are performed using the Portable SIP unit.

a Thoma cell with an optical microscope (Zeiss Axio Imager Z1, Göttingen, Germany).

3.3 Experimental setup

Fig. 1 presents the experimental setup used in this study. It has been designed as a flow-through experiment to allow the SIP monitoring of the degradation of toluene in controlled conditions. The experimental column was constructed from polyvinylidene difluoride (PVDF or Kynar®) with an inner diameter of 55 mm and a length of 250 mm. This column was designed in a previous experiment to study chlorinated solvents (Iravani *et al.* 2020). In practice, PVDF is generally used in applications requiring resistance to certain solvents because of its highly non-reactive properties (Schweitzer 2004). Here, PVDF is used to prevent toluene adsorption. Furthermore, all tubes and connectors used for pore fluid circulation are either made of tetrafluoroethylene to prevent the adsorption of toluene or from Pharmed® BPT (Bio-Pharmaceutical Tubing) to withstand pressure from the peristaltic pump actions.

The column was equipped with current injection and potential electrodes (Fig. 1). Two circular meshed stainless steel (316 L) plates, of 55 mm diameter, placed at both ends of the column, were used for current injection. This specific type of stainless steel was used to prevent oxidation due to the high salinity of the growth medium solution, and to have a homogeneous 1-D current flow in the column. Moreover, four non-polarizable custom-made $Cu/CuSO_4$ potential electrodes (adapted from Maineult *et al.* 2004) with regular spacing of 27 mm were installed along the height of the column and in between the current electrodes. These potential electrodes were named from 1 to 4 following the fluid circulation direction in the column meaning from bottom to top. In total, three measurement dipoles were made with each of the four consecutive electrodes (1–2, 2–3 and 3–4).

To maintain the purity of the bacterial strain, the column, its top and bottom caps and all fittings were autoclaved before the start of the experiment. Electrodes were disinfected with 90 per cent ethanol and rinsed with autoclaved deionized water.

SIP measurements were acquired by using a four-electrode configuration separating potential from current electrodes. These measurements were taken with a PSIP (Portable Spectral Induced Polarization) laboratory unit (Ontash and Ermac Inc., NJ). In this study, spectral acquisition of complex impedance (through amplitude $|Z|$ and phase φ) was controlled to sweep from 1 mHz to 1 kHz with 31 evenly spaced logarithmic intervals. σ' and σ'' of the complex conductivity are determined from eqs. (2) and (3).

For this work, the geometrical factor k was determined experimentally by successively filling the sample holder with solutions of sodium chloride (NaCl) with various known electrical conductivities: 46, 450 and 4150 µS cm^{-1}. The mean value was computed from all dipoles and found to be $k = 0.081$ m $\pm$ 0.002. In the electrode configuration used in this study, since the current lines are parallel close to the potential electrodes, the geometric factor can be calculated as the ratio between the column cross-sectional area A (m^2) and the distance between the potential electrodes L (m) (Binley & Kemna 2005): $k = A/L$. It has been found that A/L is equal to 0.088 m. The difference between theoretical and experimental values of k is very low (7.9 per cent). The experimentally determined factor value was used in this work.

3.4 Experimental procedure

The washed, dried and autoclaved sand was carefully placed into the sample holder in a sterile manner under the sterile atmosphere provided by two Bunsen burners. The filling procedure was conducted in seven layers to ensure even compaction and homogeneity of the porosity. For each layer, the operator gently tapped each of the four sides of the column seven times. Sand porosity was estimated

by calculating the weight difference before and after saturating the column. The porosity was found to be 34.1 per cent ± 0.4 per cent ($n = 2$). This porosity value is consistent with other studies on similar sand texture (Garba *et al.* 2019).

Subsequent to the determination of the porosity, the column was flushed several times with autoclaved deionized water and finally with a fresh growth medium. Then, the highly concentrated bacterial solution (described in Section 2.2) was circulated within the porous medium (day 0). Circulation was ensured by a peristaltic pump at a fixed rate of 0.3 mL min^{-1} for two days which is equivalent to 4 pore volumes. This step marked the inoculation phase. Its aim was to allow for the bacterial colonization of the porous medium. Thereafter, began the post-inoculation phase which consisted of continuously injecting fresh growth medium with dissolved toluene. This phase lasted around 9 d.

Throughout this experiment, oxygenation of the solution was achieved by bubbling pressurized air (0.5 bar) directly into the solution through a 0.22 μm filter while maintaining constant homogenization using a magnetic stir bar (Fig. 1).

3.5 Influent and effluent analysis

During this experiment, we employed SIP to monitor the evolution of electrical properties and paired it with a suite of chemical sensors to track key parameters (pH, σ_w, dissolved oxygen and toluene concentration) at both the inlet and outlet of the column. These combined data sets were then interpreted to infer the progression of biodegradation processes. pH and σ_w were measured using probes (WTW of Xylem Analytics, Germany) and dissolved oxygen with a PSt3 oxygen sensor spots (PreSens Precision Sensing, Germany). Toluene concentration measurement is explained in the next section (Section 3.6).

To ensure precise temporal monitoring, electrical measurements were conducted consecutively across a spectrum from 1 mHz to 1 kHz, with a complete sweep of the spectrum taking about 5 hr. This means that the time interval between successive data points at a given frequency is 5 hr. At the outlet, pH, fluid conductivity and toluene concentration sampling were automated. Specifically, pH and fluid conductivity are sampled every 2 hr, and toluene concentration every 8 hr. In contrast, inlet measurements, dissolved oxygen and SIP could not be automated and were therefore conducted manually, resulting in a less frequent measurement interval for these parameters. A summary of key experimental events and timeline is provided in Table 2.

In addition, microscope observation was carried out periodically, on the one hand, and as a first approach to evaluate the cultured bacteria purity and absence of contamination by other species in the effluent (Tindall *et al.* 2010). On the other hand, to assess qualitatively bacterial abundance in the column. It is important to note that effluent bacterial concentrations reflect only the planktonic (unattached to solid grains) fraction of the microbial population or those that have detached from biofilm. In open-flow systems like ours, planktonic cells are constantly washed out by the fluid, whereas the majority of bacterial biomass likely resides as surface-attached biofilms within the porous medium (Moore-Ott *et al.* 2022). Observations were realized at 40× objective with an optical microscope (Zeiss Axio Imager Z1, Göttingen, Germany).

3.6 Toluene concentration measurement

Toluene concentration was measured using gas chromatography–mass spectrometry in headspace mode (Shimadzu, Kyoto, Japan).

Table 2. Summary of (a) experimental timeline, (b) monitoring frequencies and (c) initial conditions.

(a)	
Experimental phases	**Day**
Beginning of inoculation phase	day 0
End of inoculation phase/Beginning of post-inoculation	day 1.5
Addition of injecting toluene	day 5
End of experiment	day 11
(b)	
Electrical and geochemical measurement	**Frequency**
SIP	1×/5 hr
pH, fluid conductivity	1×/2 hr
Toluene	1×/8 hr
c)	
Initial parameters (@$t = 0$ s)	**Value**
Porosity	34.1 per cent
Bacterial concentration	2×10^{10} bacteria mL^{-1}
Toluene concentration in bacterial solution	25 mg L^{-1}

Headspace gas chromatography–mass spectrometry (HS-GCMS) was used to detect and quantify toluene in liquid samples. This technique allows for the analysis of volatile organic compounds in the vapour phase equilibrated with the sample matrix. Detailed descriptions of the method can be found in Vilas-Boas *et al.* (2024) and related literature.

GC-MS analysis was performed on a Shimadzu GC-2010 Plus gas chromatogram equipped with a 60 m column (length: 60 m, diameter: 0.25 mm, thickness: 0.25 μm, Rxi®-624 Sil MS). Effluent samples (5 mL) were collected in amber glass vials with screw caps (10 mL). A gradient temperature programme was used for volatiles analysis; oven temperature was kept first at 40 °C for 3 min, then increased to 220 °C at a rate of 15 °C min^{-1}, and finally ramped at a rate of 20 °C min^{-1} to 260 °C and kept at this temperature for 1 min. Helium was used as the gas carrier, at a flow rate of 2.71 mL min^{-1}. The peak identification was performed using a quadruple mass-spectrometer Shimadzu QP2020 directly attached to the GC system. The interface and the ion source temperatures were both set at 200 and 280 °C, respectively. The mass spectrometer was operated at 70 kV.

Quantification of toluene concentration was calculated using a standard calibration curve prepared at serial dilutions analysed under the same HS-GCMS conditions. Quantitative dilutions were performed from a stock solution to prepare standard solutions of 0.04, 0.08, 0.1, 0.4, 0.75 and 1 m L^{-1} of toluene. These concentrations were obtained by diluting the appropriate volume of a pure toluene solution (99.9 per cent w/w) in deionized water. The standard calibration curve for the toluene standard was found to be linear over this concentration range (0.04, 0.08, 0.1, 0.4, 0.75, 1 m L^{-1}) with a correlation coefficient of 0.998.

The limits of detection (LOD) and quantification (LOQ) were evaluated as follows:

$$\mathrm{LOD} = (3 \times \gamma)/s \tag{11}$$

$$\mathrm{LOQ} = (10 \times \gamma)/s, \tag{12}$$

where γ is the standard deviation of blank samples (baseline noise) and s the slope of the calibration curve of toluene for the low concentrations (here 1 to 10 μg L^{-1}). Based on these calculations, the LOD was evaluated at 0.047 μg L^{-1} and the LOQ at 0.157 μg L^{-1}.

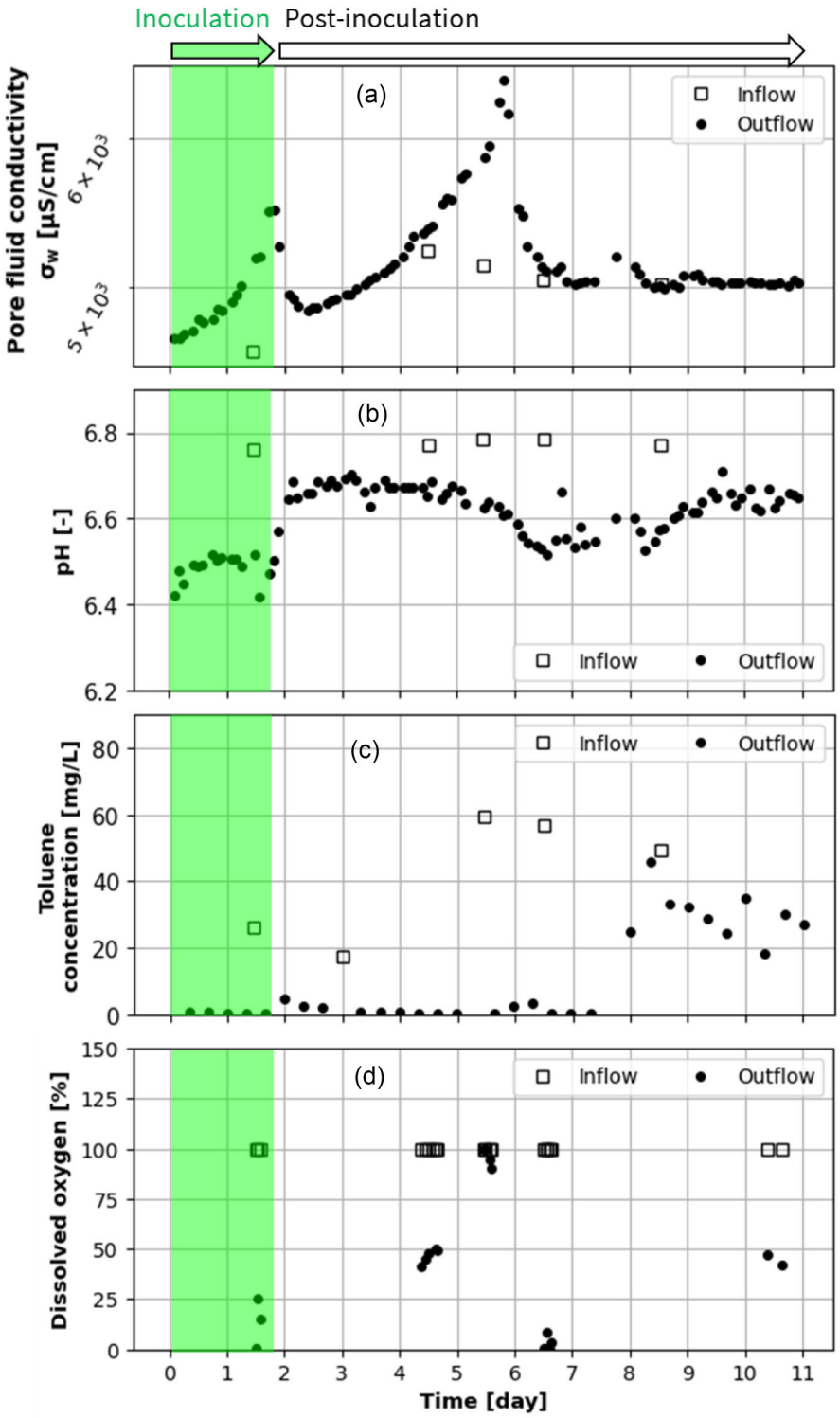

Figure 2. Monitoring of (a) electrical conductivity of the solutions, (b) pH, (c) toluene concentration and (d) dissolved oxygen, in the inflow and outflow fluid of the column throughout the experimental period. Unfilled square markers indicate measurements of the inflow and filled circles of the outflow.

Potential sources of error are related to dilutions of analysed samples, as concentrations were much higher in samples compared to the LOD and LOQ of the analytical method. This was tempered by preparing and analysing at the same time large amounts of experimental samples.

4 RESULTS

4.1 Geochemical monitoring

The figures below illustrate the temporal monitoring of σ_w (Fig. 2a), pH (Fig. 2b), toluene concentration (Fig. 2c) and dissolved oxygen

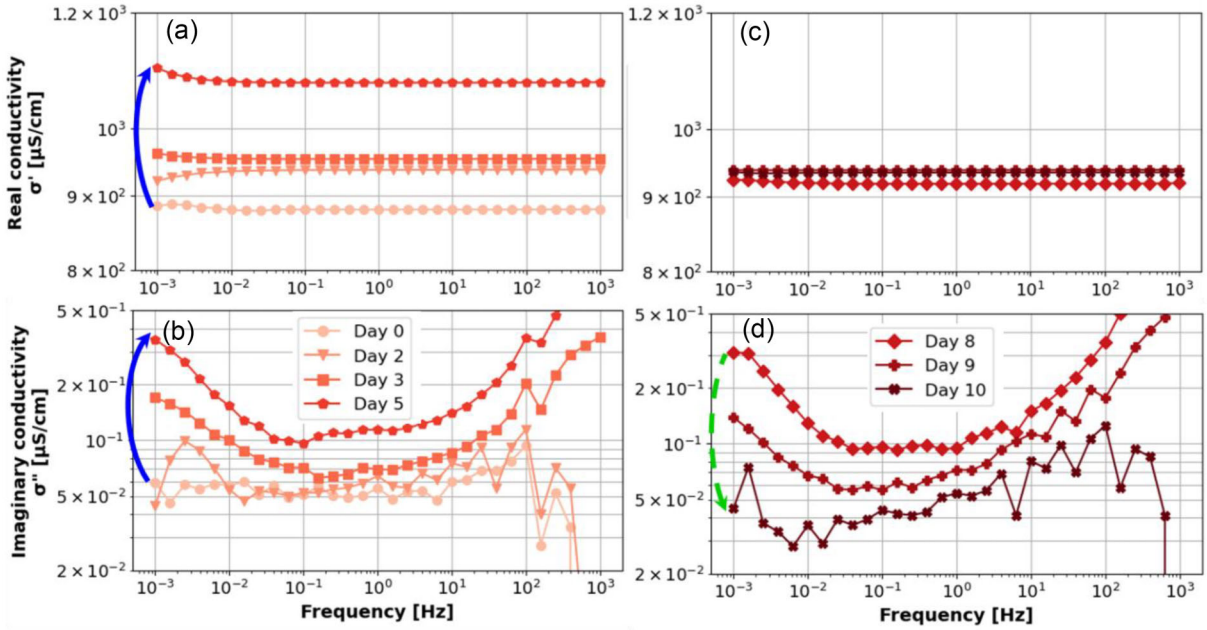

Figure 3. Real (a, c) and imaginary (b, d) conductivity spectra of dipole 1 at selected days. Panels (a–b): signal growth phase (days 0–5); panels (c–d): signal decline phase (days 8–10). Blue and green arrows indicate signal increase and decrease, respectively.

(Fig. 2d) at the inlet and outlet of the column. The inoculation and post-inoculation phases are indicated on top of each figure.

During the inoculation phase (i.e. the green backgrounds in Fig. 2), there was an increase in σ_w rising from 4700 to 5490 μS cm^{-1}. This was followed by a decrease to match the inlet solution conductivity value (4850 μS cm^{-1}) on day 2. This decline occurred after replacing the feeding bottle with fresh growth medium with dissolved toluene solution, effectively rinsing the column of the previous solution. pH, initially at 6.50, was raised at the end of the inoculation phase to 6.67, which was slightly below the average pH of the inlet solution at 6.77. Toluene concentration at the outlet was practically 0 mg L^{-1} while the inflow concentration was at 25 mg L^{-1}.

From day 2 to 6, the pore fluid electrical conductivity increased from 4840 to 6450 μS cm^{-1}. The toluene inflow concentration was at 20 mg L^{-1} whereas toluene concentration at the column outlet was nearly 0 mg L^{-1}. In a bioaugmented medium, the complete removal of toluene from the effluent strongly indicates active biodegradation, consistent with previous observations using the same bacterial strain under controlled conditions (e.g. Noel *et al.* 2016). On day 5, we decided to increase the concentration of toluene (Fig. 2c). The rationale for increasing the inflow toluene concentration on day 5 was to stimulate further microbial activity by providing additional substrate, especially as all of the toluene injected in the inlet (around 25 g L^{-1}) appeared to be fully consumed (outlet toluene concentration is 0 mg L^{-1}). Following this increase, the lowest dissolved oxygen concentration (0.02 per cent) was recorded in the outflow.

Between days 6 and 8, the medium acidified slightly, reaching a pH of 6.53. Similarly, σ_w declined rapidly to match that of the inlet solution. Meanwhile, the previously negligible toluene concentration, at the outlet, rose to an average of around 30 mg L^{-1} until the end of the experiment, when the oxygen reached 50 per cent.

It should be mentioned that the fluctuations observed in the inflow toluene concentration over time were due to the replacement of the feeding bottle. This was necessary as the reservoir had emptied due to continuous pumping. This change may have caused slight variability in the toluene concentration during preparation. We do not interpret these fluctuations as evidence of contamination or degradation occurring outside the column because all components of the system (bottles, tubing and column) were sterilized and tightly controlled throughout the experiment.

4.2 Real and imaginary conductivity

4.2.1 Spectral response

Figs 3(a) and (c) present the real and imaginary conductivity spectra at seven different dates. Here, for conciseness, we will focus exclusively on the results from dipole 1 (located at the bottom of the column). Real and imaginary conductivity spectra of dipoles 2 and 3 are available in the Supplementary Information. Overall, the real part of the conductivity shows minimal to no frequency dependency. However, it exhibits two distinct temporal phases: an initial phase of increase from 880 to 1077 μS cm^{-1} between days 0 to 5 (Fig. 3a), followed by a phase of decline to a value of 934 μS cm^{-1} on day 10 (Fig. 3c). The missing SIP data for days 6 and 7 are due to a temporary interruption in measurements over a weekend and national holiday period, which limited manual data acquisition. As SIP measurements in our setup could not be automated, no data could be collected during that time.

Figs 3(b) and (d) present the imaginary conductivity spectra at the same seven dates. Contrary to the real conductivity, the imaginary conductivity spectra show frequency-dependent behaviour. From day 0 to 5 (Fig. 3b), at low frequencies (below 10^{-2} Hz), we observe an increase of the imaginary conductivity whose amplitude reaches its maximum value of 0.35 μS cm^{-1} on day 5. It might be possible that the complete polarization peak could be observed if the measurements had covered lower frequencies, specifically below 1 mHz (i.e. below the instrumental range limit). Following day 6, after the increase in the concentration of toluene injected into the column, the amplitude at low frequencies (Fig. 3d) gradually decreased and approached 0.05 μS cm^{-1}.

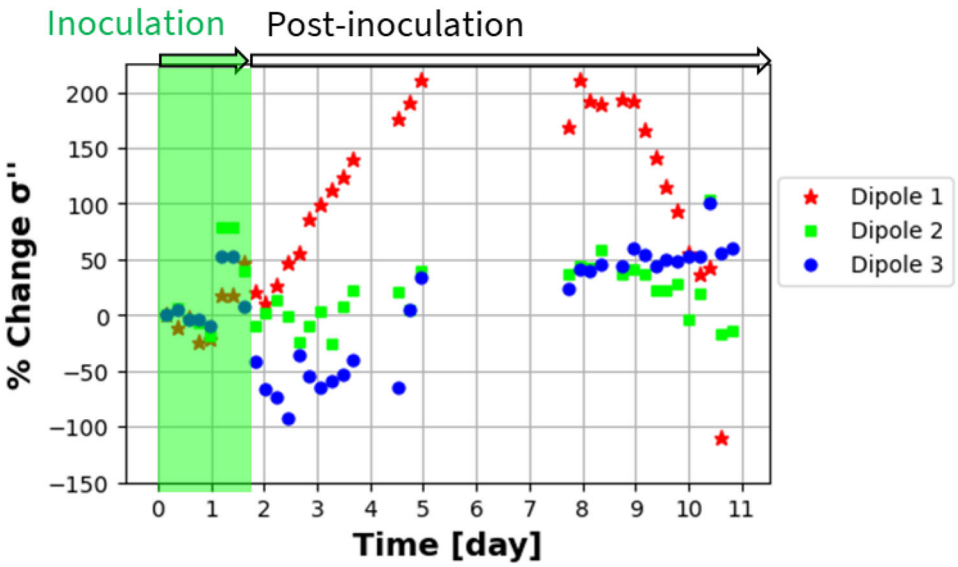

Figure 4. Percent variation of the imaginary part of the conductivity (at 1.5 mHz) in the column. The graph shows dipoles 1, 2 and 3, placed at heights 111.5, 138.5 and 165.5 mm, respectively, from the bottom to the top of the column.

4.2.2 Relative change of imaginary conductivity at one frequency in time

We selected 1.5 mHz as a reference for highlighting the temporal changes of the imaginary conductivity in this experiment. Following the recommendation of Rosier *et al.* (2019a), we expressed the SIP response σ'' as a relative change $\Delta\sigma''$ to the geometric mean of the bacterial evolution, multiplied by a reference value σ''_{ctrl},

$$\Delta\sigma'' = \frac{\sigma'' - \sigma''_{\text{ctrl}}}{\sqrt{\sigma'' \times \sigma''_{\text{ctrl}}}}. \quad (13)$$

This reference (σ''_{ctrl}) is the SIP signature of the sand column at the end of the inoculation phase. The authors explained that using the geometric mean mitigates the influence of large variations in data sets, unlike the arithmetic mean, which often leads to overestimations.

Fig. 4 shows the temporal evolution of $\Delta\sigma''$ expressed in percentage. During the inoculation phase, dipoles 2 and 3 showed the same trends as dipole 1, with an increase in the electrical signal from the start of the experiment up to a maximum variation of 50 per cent, followed by a decrease to 0 per cent on day 2. This decrease could be explained by the loss of planktonic bacteria after inoculation ceased and the introduction of a fresh growth medium with dissolved toluene. Such a pattern is typical for microorganisms (with submicron sizes) in open-flow systems, where cells are carried by the circulating fluid (Wheeler *et al.* 2019). Indeed, between days 2 to 6, all dipoles exhibited different trends. Dipole 3′s per cent variation decreased quickly, stabilizing around −50 per cent. In contrast, dipole 2 showed relatively minimal change during this period. Nevertheless, both dipoles experienced an increase, reaching 47 per cent on day 5. Dipole 1 showed the most substantial increase, with its variation percentage rising from 0 to 200 per cent.

Following the increase in toluene concentration introduced on day 5, the per cent change in imaginary conductivity at dipole 1 appeared to have entered a stationary phase until day 9, after which the per cent change in imaginary conductivity began to decrease. However, due to the absence of SIP data between days 5 and 7, the exact evolution of the signal during this period remains uncertain. In contrast, dipoles 2 and 3 showed no major changes during this time.

4.3 Effluent bacterial density and biofilm production

Figs 5(a) and (b) show bacteria content in the effluent on day 2 and day 10, respectively. In Fig. 5(a), bacteria are observed in individual form. These individuals exhibited elongated shapes. Based on previous observations, this shape is characteristic of the *R. wratislaviensis* strain. The absence of other bacterial forms tends to confirm that only one bacterial strain was present at the end of the inoculation phase. Compared to Fig. 5(a), the observation at day 10 (Fig. 5b) shows a significant decrease in the bacterial population present in the effluent. This can be related to a decrease in the bacterial population inside the column. Indeed, a similar flow-through experiment conducted by Joo *et al.* (2021) revealed in their experiment that the bacterial content inside the column follows the same trend as that in the effluent.

To characterize effective colonization of the grain surfaces inside the column, we renewed the experiment of this study following the same protocol and conditions (see Table 2). The experiment was run maintaining a constant toluene concentration of 25 mg L^{-1} over one week. Then, sand grains were sampled on day 5 for CryoSEM (Cryo-Scanning Electron Microscopy) observation (Fig. 6).

CryoSEM imaging showed bacterial cells attached to sand grains (Fig. 6). The biofilm is identified as a diffuse, amorphous material with a smooth and less defined texture compared to the mineral grains or bacterial cells. It lacks distinct cellular boundaries and displays a gelatinous morphology typical of extracellular polymeric substances secreted by bacteria. However, biofilm production during this experiment has only been limited to a thin layer around the grains potentially with no bioclogging effects. This limited biofilm development is supported by comparison with Environmental Scanning Electron Microscopy images from Joo *et al.* (2021; their fig. 4), where biofilms are clearly visible without magnification and bioclogging confirmed. In contrast, in our study, higher magnification was required to observe biofilm presence, indicating a much less developed structure.

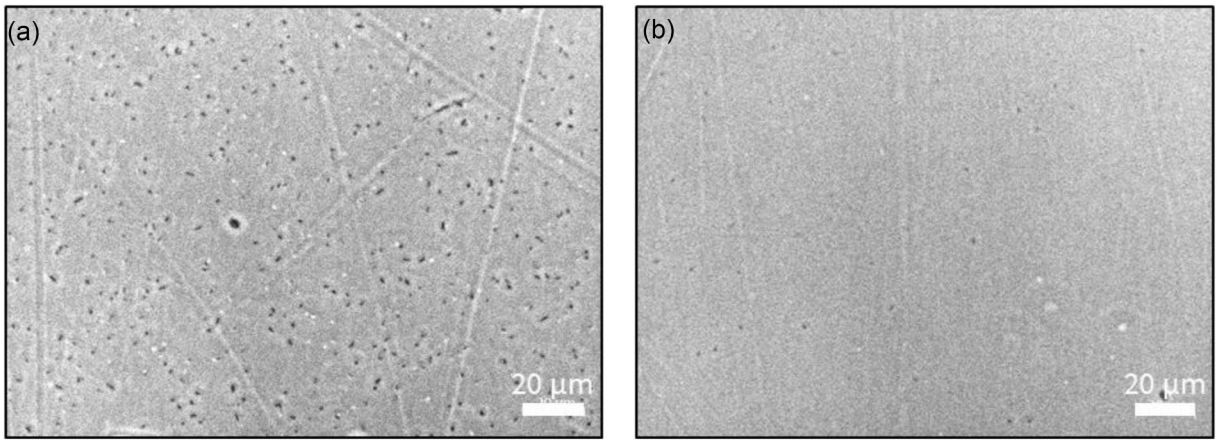

Figure 5. Representative optical microscope observation of the outflow on the (a) second and (b) tenth days showing bacterial abundance in the effluent.

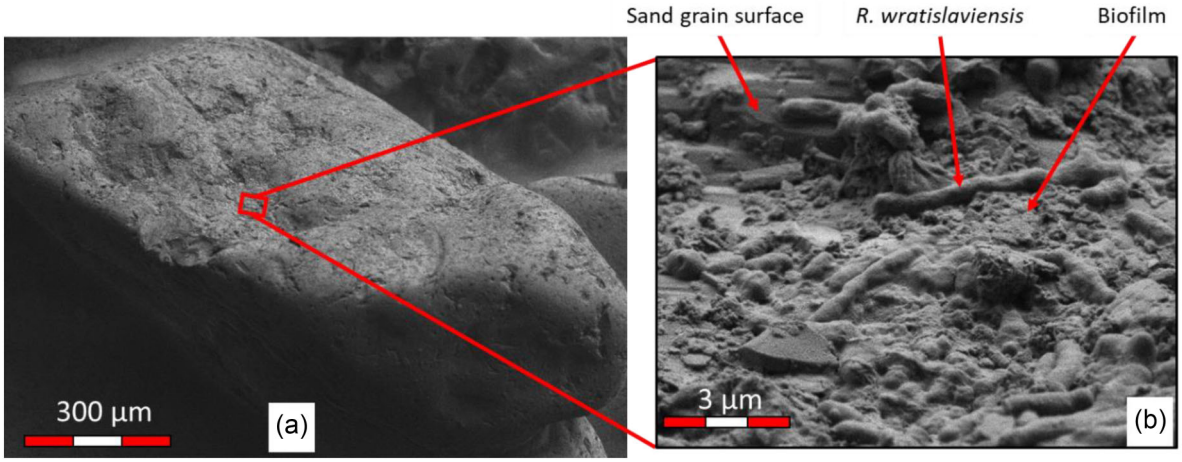

Figure 6. (a) Cryo-SEM image of a sand grain sampled on day 5 from a replicate experiment under identical conditions. (b) Magnification on the surface of the sand grain to observe bacterial cells in a thin biofilm coating.

5 DISCUSSION

5.1 Biodegradation dynamics of toluene

CryoSEM imaging confirmed bacterial growth and biofilm formation on grains (Fig. 6). In the column, *R. wratislaviensis* biodegrades toluene, which is confirmed by the absence of toluene at the column outlet (Fig. 2c). Toluene biodegradation results in an increase in fluid electrical conductivity. This increase is due to the rise in ionic strength of the culture solution, resulting from the numerous metabolites generated during the transformation of toluene molecules by microorganisms (e.g. Kessouri *et al.* 2019).

Between days 6 and 8, an increase in bacterial activity was observed, evidenced by a more pronounced acidification of the outlet solution (Fig. 2b), the absence of toluene (Fig. 2c), and heightened respiratory activity reflected by low-dissolved oxygen levels (Fig. 2d). This intensified bacterial activity was triggered by the injection of a larger amount of toluene on day 5. Following this phase of heightened activity, a decrease in the variation of imaginary conductivity was observed, suggesting a reduction in bacterial concentration within the column. The biogeochemical mechanisms underlying this phenomenon will be explained in the subsequent paragraphs.

Toluene degradation occurs through the oxidation of carbon bonds, which requires the availability of oxygen atoms supplied by dissolved oxygen in the culture medium. The biodegradation or chemical transformation of toluene follows several degradation pathways in which electrons or hydrogen atoms are transferred from the molecule (or its metabolites) to molecular oxygen (O_2) (Hayaishi, 2005). The incorporation of molecular oxygen into various organic compounds is facilitated by enzymes known as oxygenases, which catalyse the addition of oxygen across a double bond between two carbon atoms of the substrate (Krivoruchko *et al.* 2023). To support aerobic biodegradation, oxygen demand can be considerably high (Fragkou *et al.* 2021) as seen in oxygen consumption after the increase in toluene concentration. *R. wratislaviensis* is aerobic and cannot sustain prolonged anoxic stress conditions (Kuyukina & Ivshina 2019). This situation is the cause of the mortality of part of the bacteria.

On another note, the partial mortality of bacteria is not interpreted as a consequence of toluene toxicity because of complementary batch experiments. In these batch experiments (results not shown in this paper), toluene at the tested concentrations (25 to 200 mg L^{-1}) did not exhibit toxic effects on *R. wratislaviensis*. Based on this work, the observed reduction in toluene removal is more plausibly attributed to oxygen limitation rather than substrate toxicity or nutrient deficiency.

Acidification occurred because the final degradation step of toluene generates CO_2 molecules (mineralization). In an aqueous

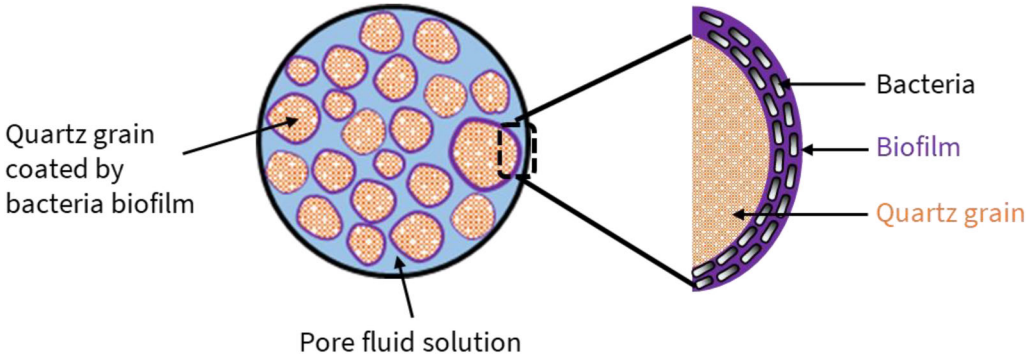

Figure 7. Conceptual diagram of the polarization mechanism associated with biofilm growth on grain surfaces. As bacteria form a biofilm, an EDL develops at the interface, similar to mechanisms observed in clay coatings.

state, these molecules dissociate into H^+ and HCO_3^- ions under specific conditions (particularly when pH is between 6 and 8), thus acidifying the environment. Previous studies (Abdel Aal *et al.* 2004; Atekwana *et al.* 2006) have also reported pH decreases during hydrocarbon mineralization.

While the reduction in toluene concentration in the effluent, the drop in pH, the oxygen depletion and the effective colonization of bacteria on sand grains from Cryo-SEM images collectively suggest biodegradation, we acknowledge that direct monitoring of bacterial evolution or the detection of metabolic by-products, were not obtained. Therefore, our interpretation of SIP signals as markers of microbial activity and degradation remains a plausible hypothesis supported by indirect evidence, but not confirmed.

Between day 1 and day 2, which marked the end of the inoculation phase, the imaginary conductivity per cent change decreases from 50 to 0 per cent on all three dipoles. This decline can be explained by the fact that planktonic cells (bacteria that have not attached to the sand grains) are rinsed out of the column with the injection of a fresh growth solution. Consequently, part of the bacterial contribution is lost. The same evolution has been observed by Noel *et al.* (2016) who also worked on aerobic biodegradation of toluene using the same strain of bacteria. It is important to note that, under our flow conditions, one pore volume is replaced every 13 h which allows SIP monitoring of this event as seen from Fig. 4.

However, as bacterial cells develop inside the column as biofilms (see Fig. 6), no clear polarization peak is present over the whole spectrum. The presence or absence of a bacterial polarization peak attributed to bacterial presence varies across studies in the SIP literature. Studies such as Zhang *et al.* (2014), Rosier *et al.* (2019) and Joo *et al.* (2021) reported bacterial polarization peaks appearing between 0.05 and 10 Hz, while others such as Saneiyan *et al.* (2024) note no prominent bacterial peak which is the case in this study. This suggests that the polarization mechanism of *R. wratislaviensis* in the culture medium of this experiment may differ from those observed in the referenced studies.

In fact, we think that the absence, in the measured frequencies, of a polarization peak is the result of two contributing factors: the relatively high salinity of the nutrient solution and the limited biofilm production by the bacteria. The elevated conductivity of the medium ($\sim$6 mS cm^{-1}) likely attenuates the SIP signal. At high salinity, the diffuse layer of the electrical double layer, responsible for restricting the transport of co-ions, is compressed, which reduces co-ions blocking and consequently diminishes the polarization effect (Vinegar & Waxman 1984; Slater & Lesmes 2002). Additionally, the polarization mechanism is likely connected to the formation of an EDL around the sand grains, induced by the presence of a biofilm partially or fully covering their surfaces. A schematic diagram is provided to illustrate the possible polarization source mechanism associated with the formation of a biofilm (Fig. 7). This mechanism closely resembles the model described for clay minerals that form coatings around sand grains (De Lima & Sharma 1990). Considering the following equation, which relates the average size of the polarizing objects a in the column to the relaxation time $\tau = a^2/2D$, via a diffusion coefficient D (m^2 s^{-1}), and assuming $a = 1$ mm (median radius of the sand grain placed in the column) and $D = 10^{-9}$ m^2 s^{-1}, we found that the corresponding polarization frequency is 3 mHz. This first approximation confirms the observed results and is supported by the recent work of Song *et al.* (2024). In this work, the authors demonstrated that SIP is more sensitive to bacterial microcolonies than to individual bacterial cells.

The low-biofilm production behaviour of *R. wratislaviensis* stands in contrast to that of *Rhodococcus ruber*, another species from the *Rhodococcus* genus. Studies on the latter have demonstrated a strong preference for a biofilm mode of growth (Sivan *et al.* 2006). Indeed, SEM observations characterizing biofilm production in their research reveal a tendency towards cell aggregation, even in liquid culture (Orr *et al.* 2004). Our study suggests that an individual cell growth pattern with limited biofilm production may be the preferential mode of development for *R. wratislaviensis*. Besides, reductions in charge transport caused by bioclogging have been identified as a significant source of polarization at low frequencies (Abdel Aal *et al.* 2004; Davis *et al.* 2006; Atekwana & Slater 2009; Joo *et al.* 2021). These findings highlight the importance of microbial growth forms in influencing geophysical signals during biodegradation processes.

5.2 Bacterial evolution predicted using the model of Revil *et al.* (2012)

We used the approach proposed by Revil *et al.* (2012) to infer the growth and decay rate of bacteria in porous sand from time-lapse SIP. We also made the choice to only fit data from dipole 1 which shows significant variation in imaginary conductivity (see Fig. 5). This decision is based on the expectation that bacterial abundance would be highest in the lower part of the column due to its proximity to the nutrient solution entry point (e.g. Mellage *et al.* 2015). Following the assumption by Revil *et al.* (2012), we made the assumption that in time-lapse, the change in imaginary conductivity reflects a direct change in bacterial concentration.

Fig. 8(a) shows the time-lapse evolution of the imaginary conductivity of dipole 1 at a frequency of 1.5 mHz, along with the fitted

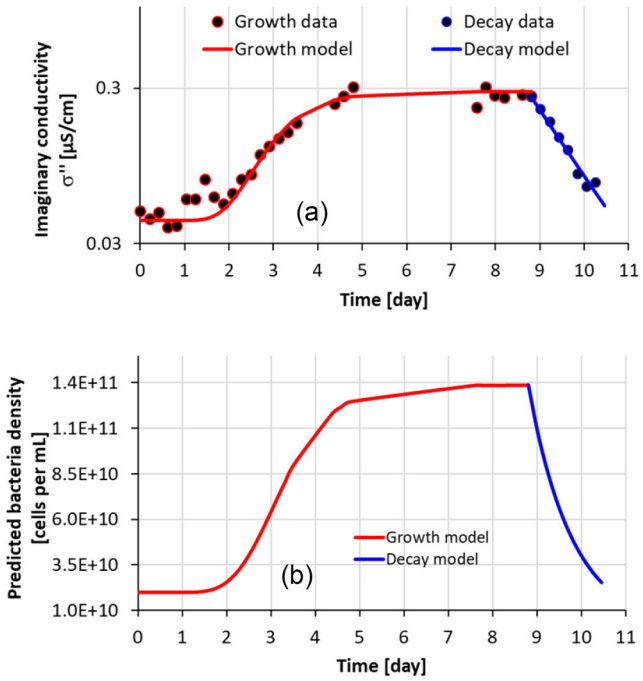

Figure 8. (a) Fit of the models to the growth and decay stages of bacterial development to the imaginary conductivity of dipole 1 at a frequency of 1.5 mHz. (b) Predicted bacterial evolution in the column from the calibrated parameters.

models. By applying the least-squares fitting criteria to these equations, the following parameter values were obtained: $'= 4.25.10^{-2}$ µS cm^{-1}; $\sigma_B^{M''} = 2.84.10^{-1}$ µS cm^{-1}; $\mu_m = 1$ d^{-1}; $\tau = 1$ d and $k_d = 1$ d^{-1}. Based on these parameter values, and taking an initial bacterial concentration of 2×10^{10} bacteria mL^{-1}, we predicted the bacterial evolution below in the column (Fig. 8b). Notably, the imaginary conductivity measured on day 10 remains slightly higher than on day 2 (see Fig. 8a). Since the growth model is fitted to the temporal evolution of imaginary conductivity, this observation justifies the slightly elevated estimated bacterial density at day 10.

Our fitted parameters are consistent with other studies on the aerobic biodegradation of toluene. Choi *et al.* (1992) and Vecht *et al.* (1988) reported values for μ_m of 1.2 and 3.1 d^{-1}. Alvarez *et al.* (1991) found a lag phase τ of 1 to 2 d, without specifying exactly the value. As for Pedersen *et al.* (1997), they reported a specific decay rate k_d of 1.15 d^{-1}. However, it needs to be pointed out that studies such as Ostendorf *et al.* (2007) on the biodegradation of hydrocarbons found different values to those mentioned in this paper: μ_m and k_d between 0.02 to 0.32 d^{-1} and 0.05 to 0.1 d^{-1}. In fact, intrinsic values of Monod's model or reparametrized model to study biodegradation such as Zwietering *et al.* (1990) are highly specific to the strain and growth conditions (Alvarez *et al.* 1991). In this context, one has to exert caution in comparing values from different studies.

6 CONCLUSION

In this study, a laboratory experiment was conducted to monitor and characterize the biodegradation of toluene in a porous medium using SIP. The results confirm the potential of SIP as a sensitive tool for monitoring the biodegradation processes of toluene (BTEX), particularly at low frequencies. However, it is important to note that translating this sensitivity to the field remains challenging, as achieving the required measurement precision (i.e. below 0.1 mrad) in noisy environmental settings is difficult. It is likely that the maximum polarization frequency of *R. wratislaviensis* lies below 1 mHz under the growth conditions used in this study. However, the relatively weak amplitude of the imaginary conductivity response suggests that the strain's limited biofilm-forming ability also played a major role in controlling the overall imaginary conductivity response.

To quantify these observations, the bacterial growth and decay models proposed by Revil *et al.* (2012) were employed in this study. The model predicted bacterial dynamics based on SIP measurements and fitted parameters, supporting the possibility of integrating SIP with predictive modelling for *in situ* biodegradation monitoring. These results pave the way for more accurate and non-invasive methods to assess microbial activity in contaminated environments, providing valuable insights for sustainable remediation strategies.

In terms of potential improvements, it could be beneficial to provide an additional nutrient source for the bacteria beyond just toluene. While some bacteria are capable of using toluene as a carbon source, this compound remains challenging to degrade. Enriching the culture medium with an alternative carbon source, such as glucose, could enhance biostimulation and improve the system's biodegradation capacity (Roy *et al.* 2018; Fragkou *et al.* 2021).

As for a more efficient way of oxygenating the bacterial solution, other methods such as addition of water peroxide could boost fluid oxygenation.

From a methodological perspective, it is also important to acknowledge certain limitations. Conducting time-lapse measurements at very low frequencies, such as 1 mHz or below, presents significant constraints due to the lengthy acquisition time required. This approach may not be suitable for monitoring processes with rapid dynamics, which should be considered when contextualizing these results for real-time field-scale bioremediation applications. Furthermore, it becomes obvious from the results of this study that the choice of bacterial strain for biodegradation applications is a critical factor, as it directly influences the effectiveness and feasibility of the process.

ACKNOWLEDGMENTS

This research was funded by the French Research Agency (IMAGE project, grant number #ANR-21-CE04-0013) and the French Geological Survey. The authors express their gratitude to IFP Énergies Nouvelles (IFPEN) for supplying the *Rhodococcus wratislaviensis* strain. Warm thanks are also extended to Isis Fourment, Aya Nianzou, Hafida Tris and Mickael Charron for their various assistance during the experimental setup and execution. We are grateful to Philippe Leroy for his insightful discussions throughout the drafting of this manuscript. Lastly, the authors thank the editor, Sina Saneiyan, Dimitrios Ntarlagiannis and one anonymous reviewer for their comments that helped us to improve the manuscript.

SUPPORTING INFORMATION

Supplementary data are available at *GJIRAS* online.

Figure S1: Real conductivity spectra of dipole 1 at seven different dates.
Figure S2: Real conductivity spectra of dipole 2 at seven different dates.
Figure S3: Imaginary conductivity spectra of dipole 1 at seven different dates.

Figure S4: Imaginary conductivity spectra of dipole 2 at seven different dates.
Figure S5: Resistivity magnitude and phase shift of the three dipoles measured on tap water (450 μS cm^{-1}) at the end of the experiment.
Please note: Oxford University Press is not responsible for the content or functionality of any supporting materials supplied by the authors. Any queries (other than missing material) should be directed to the corresponding author for the paper.

CONLFICT OF INTEREST

None.

DATA AVAILABILITY

The data set for this manuscript is available at https://doi.org/10.5281/zenodo.17735717.

REFERENCES

Abdel Aal, G.Z., Atekwana, E.A., Slater, L.D. & Atekwana, E.A., 2004. Effects of microbial processes on electrolytic and interfacial electrical properties of unconsolidated sediments, *Geophys. Res. Lett.,* **31,** L12505.

Abdel Aal, G.Z., Slater, L.D. & Atekwana, E.A., 2006. Induced-polarization measurements on unconsolidated sediments from a site of active hydrocarbon biodegradation, *Geophysics,* **71,** H13–H24.

Alvarez, P.J., Anid, P.J. & Vogel, T.M., 1991. Kinetics of aerobic biodegradation of benzene and toluene in sandy aquifer material, *Biodegradation,* **2,** 43–51.

Archie, G.E., 1942. The electrical resistivity log as an aid in determining some reservoir characteristics, *Trans. AIME,* **146,** 54–62.

Atekwana, E.A. & Slater, L.D., 2009. Biogeophysics: a new frontier in Earth science research, *Rev. Geophys.,* **47,** RG4004.

Atekwana, E.A., Werkema, D.D. & Atekwana, E.A., 2006. Biogeophysics: the effects of microbial processes on geophysical properties of the shallow subsurface, *Appl. Hydrogeophysics,* pp. 161–193, eds, Vereecken, H., Binley, A., Cassiani, G., Revil, A. & Titov, K., Springer, Netherlands.

Auffret, M., Labbé, D., Thouand, G., Greer, C.W. & Fayolle-Guichard, F., 2009. Degradation of a mixture of hydrocarbons, gasoline, and diesel oil additives by *Rhodococcusaetherivorans* and *Rhodococcuswratislaviensis*, *Appl. Environ. Microb.,* **75,** 7774–7782.

Ball, A. & Truskewycz, A., 2013. Polyaromatic hydrocarbon exposure: an ecological impact ambiguity, *Environ. Sci. Pollut. Res.,* **20,** 4311–4326.

Ben Moshe, S., Kessouri, P., Erlich, D. & Furman, A., 2021. Geophysically-based analysis of BTCs and ion exchange processes in soil, *Hydrol. Earth Syst. Sci.,* **25,** 3041–3052.

Berne, C., Ellison, C.K., Ducret, A. & Brun, Y.V., 2018. Bacterial adhesion at the single-cell level, *Nat. Rev. Micro.,* **16,** 616–627.

Binley, A. & Kemna, A., 2005. DC resistivity and induced polarization methods, in *Hydrogeophysics: Water Science and Technology Library,* Vol. **50,** pp. 129–156, eds., Rubin, Y. & Hubbard, S.S., Springer, Netherlands.

Buchanan, R.E., 1918. Life phases in a bacterial culture, *J. Infect. Dis.,* **23,** 109–125.

Carreón-Rodríguez, O.E., Gosset, G., Escalante, A. & Bolívar, F., 2023. Glucose transport in *Escherichia coli*: from basics to transport engineering, *Microorganisms,* **11,** 1588.

Chikere, C.B., Okpokwasili, G.C. & Chikere, B.O., 2011. Monitoring of microbial hydrocarbon remediation in the soil, *3 Biotech,* **1,** 117–138.

Choi, Y., Lee, J. & Kim, H., 1992. A novel bioreactor for the biodegradation of inhibitory aromatic solvents: experimental results and mathematical analysis, *Biotechnol. Bioeng.,* **40,** 1403–1411.

Davis, C.A., Atekwana, E., Atekwana, E., Slater, L.D., Rossbach, S. & Mormile, M.R., 2006. Microbial growth and biofilm formation in geologic media is detected with complex conductivity measurements, *Geophys. Res. Lett.,* **33**.

De Lima, O.A.L. & Sharma, M.M., 1990. A grain conductivity approach to shaly sandstones, *Geophysics,* **55,** 1347–1356.

De Souza, E.S., Becker, B.R., Vieira-da-Motta, O. & Almeida, J.C.D.A., 2024. Oil spill bioremediation strategies in Brazilian tropical seawater—The role of polycyclic aromatic hydrocarbons degradation, *CLEAN—Soil Air Water,* **52,** 2300 081.

Dove, P.M. & Elston, S.F., 1992. Dissolution kinetics of quartz in sodium chloride solutions: analysis of existing data and a rate model for 25°C, *Geochim. Cosmochim. Acta,* **56,** 4147–4156.

Fragkou, E., Antoniou, E., Daliakopoulos, I., Manios, T., Theodorakopoulou, M. & Kalogerakis, N., 2021. In situ aerobic bioremediation of sediments polluted with petroleum hydrocarbons: a critical review, *J. Mar. Sci. Eng.,* **9,** 1003.

Garba, M.A., Vialle, S., Madadi, M., Gurevich, B. & Lebedev, M., 2019. Electrical formation factor of clean sand from laboratory measurements and digital rock physics, *Solid Earth,* **10,** 1505–1517.

Geize, R.v.d. & Dijkhuizen, L., 2004. Harnessing the catabolic diversity of rhodococci for environmental and biotechnological applications, *Curr. Opin. Microbiol.,* **7,** 255–261.

Grosse, C., 2002. Relaxation mechanisms of homogeneous particles and cells suspended in aqueous electrolyte solutions, in *Interfacial Electrokinetics and Electrophoresis,* 1st edn., Vol. **106,** pp. 279–327, CRC Press.

Hayaishi, O., 2005. An odyssey with oxygen, *Biochem. Biophys. Res. Commun.,* **1,** 2–6.

Iravani, M.A., Deparis, J., Davarzani, H., Colombano, S., Guérin, R. & Maineult, A., 2020. The influence of temperature on the dielectric permittivity and complex electrical resistivity of porous media saturated with DNAPLs: a laboratory study, *J. Appl. Geophys.,* **172,** 103 921.

Joo, H.-W., Kwon, T.-H., Lee, S.-R. & Wu, Y., 2021. Relaxation behavior in low-frequency complex conductivity of sands caused by bacterial growth and biofilm formation by *Shewanellaoneidensis* under a high-salinity condition, *Geophysics,* **86,** B389–B400.

Kamranifar, M., Pourzamani, H., Khosravi, R., Ranjbar, G. & Ebrahimpour, K., 2025. Phytotoxic effects of petroleum hydrocarbons on germination and growth of the native halophyte Salicornia sinus persica in oil contaminated soil, *Sci. Rep.,* **15,** 8459.

Kemna, A. *et al.*, 2012. An overview of the spectral induced polarization method for near-surface applications, *Near Surf. Geophys.,* **10,** 453–468.

Kessouri, P. *et al.*, 2019. Induced polarization applied to biogeophysics: recent advances and future prospects, *Near Surf. Geophys.,* **17,** 595–621.

Konhauser, K., 2007. *Introduction to Geomicrobiology,* Vol. **144,** Blackwell Publishing, Carlton.

Krivoruchko, A., Kuyukina, M., Peshkur, T., Cunningham, C.J. & Ivshina, I., 2023. *Rhodococcus* strains from the specialized collection of alkanotrophs for biodegradation of aromatic compounds, *Molecules,* **28,** 2393.

Kuppan, N., Padman, M., Mahadeva, M., Srinivasan, S. & Devarajan, R., 2024. A comprehensive review of sustainable bioremediation techniques: eco friendly solutions for waste and pollution management, *Waste Manag. Bull.,* **2,** 154–171.

Kuyukina, M.S. & Ivshina, I.B., 2019. Bioremediation of contaminated environments using *Rhodococcus*, *Biol. Rhodococcus,* **16,** 231–270.

Madigan, M.T., Clark, D.P., Stahl, D. & Martinko, J.M., 2010. *Brock: Biology of Microorganisms,* 13th edn., Benjamin Cummings.

Maineult, A., Bernabé, Y. & Ackerer, P., 2004. Electrical response of flow, diffusion, and advection in a laboratory sand box, *Vadose Zone J.,* **3,** 1180–1192.

Martínková, L., Uhnáková, B., Pátek, M., Nešvera, J. & Křen, V., 2009. Biodegradation potential of the genus *Rhodococcus*, *Environ. Int.,* **35,** 162–177.

Mellage, A., Eckert, D., Grösbacher, M., Inan, A.Z., Cirpka, O.A. & Griebler, C., 2015. Dynamics of suspended and attached aerobic toluene degraders in small-scale flow-through sediment systems under growth and starvation conditions, *Environ. Sci. Technol.,* **49,** 7161–7169.

Mellage, A., Smeaton, C.M., Furman, A., Atekwana, E.A., Rezanezhad, F. & Van Cappellen, P., 2018. Linking spectral induced polarization (SIP) and subsurface microbial processes: results from sand column incubation experiments, *Environ. Sci. Technol.,* **52,** 2081–2090.

Mewafy, F.M., Werkema, D.D., Atekwana, E.A., Slater, L.D., Abdel Aal, G., Revil, A. & Ntarlagiannis, D., 2013. Evidence that bio-metallic mineral precipitation enhances the complex conductivity response at a hydrocarbon contaminated site, *J. Appl. Geophys.,* **98,** 113–123.

Mirghani, R. *et al.*, 2022. Biofilms: formation, drug resistance and alternatives to conventional approaches, *AIMS Microbiol.* **8,** 239–277.

Monod, J., 1949. The growth of bacterial cultures, *Annu. Rev. Microbiol.,* **3,** 371–394.

Moore-Ott, J.A., Chiu, S., Amchin, D.B., Bhattacharjee, T. & Datta, S.S., 2022. A biophysical threshold for biofilm formation, (R. E. Goldstein & A. M. Walczak, Eds.), *eLife,* **11,** e76380.

Nelson, D.L. & Cox, M.M., 2013. *Lehninger: Principles of Biochemistry,* 6th edn., W.H. Freeman.

Noel, C., Gourry, J., Deparis, J., Ignatiadis, I., Battaglia-Brunet, F. & Guimbaud, C., 2016. Suitable real-time monitoring of the aerobic biodegradation of toluene in contaminated sand by spectral induced polarization measurements and CO_2 analyses, *Near Surf. Geophys.,* **14,** 263–273.

Ntarlagiannis, D., Williams, K.H., Slater, L. & Hubbard, S., 2005. Low-frequency electrical response to microbial induced sulfide precipitation, *J. Geophys. Res. Biogeosciences,* **110**.

Orr, I.G., Hadar, Y. & Sivan, A., 2004. Colonization, biofilm formation and biodegradation of polyethylene by a strain of *Rhodococcusruber*, *Appl. Microbiol. Biotechnol.,* **65,** 97–104.

Ostendorf, D.W., Schoenberg, T.H., Hinlein, E.S. & Long, S.C., 2007. Monod kinetics for aerobic biodegradation of petroleum hydrocarbons in unsaturated soil microcosms, *Environ. Sci. Technol.,* **41,** 2343–2349.

Palmer, J., Flint, S. & Brooks, J., 2007. Bacterial cell attachment, the beginning of a biofilm, *J. Ind. Microbiol. Biotechnol.,* **34,** 577–588.

Pedersen, A.R., Møller, S., Molin, S. & Arvin, E., 1997. Activity of toluene-degrading *Pseudomonas putida* in the early growth phase of a biofilm for waste gas treatment, *Biotechnol. Bioeng.,* **54,** 131–141.

Peterson, B.W., Sharma, P.K., Mei, H.C.v.d. & Busscher, H.J., 2012. Bacterial cell surface damage due to centrifugal compaction, *Appl. Environ. Microbiol.,* **78,** 120–125.

Petrova, O.E. & Sauer, K., 2016. Escaping the biofilm in more than one way: desorption, detachment or dispersion, *Curr. Opin. Microbiol.,* **30,** 67–78.

Rembert, F., Fernandez, N.M., Luquot, L., Guérin, R. & Jougnot, D., 2025. Investigating solute transport and reaction using a mechanistically coupled geochemical and geophysical modeling approach, *Adv. Water Resour.,* **196,** 104 879.

Revil, A. & Glover, P.W.J., 1998. Nature of surface electrical conductivity in natural sands, sandstones, and clays, *Geophys. Res. Lett.,* **25,** 691–694.

Revil, A., Atekwana, E., Zhang, C., Jardani, A. & Smith, S., 2012. A new model for the spectral induced polarization signature of bacterial growth in porous media, *Water Resour. Res.,* **48,** W09545.

Rosier, C.L., Atekwana, E.A., Aal, G.A. & Patrauchan, M.A., 2019. Cell concentrations and metabolites enhance the SIP response to biofilm matrix components, *J. Appl. Geophys.,* **160,** 183–194.

Roy, A. *et al.*, 2018. Biostimulation and bioaugmentation of native microbial community accelerated bioremediation of oil refinery sludge, *Bioresour. Technol.,* **253,** 22–32.

Saeedi, M., Malekmohammadi, B. & Tajalli, S., 2024. Interaction of benzene, toluene, ethylbenzene, and xylene with human's body: insights into characteristics, sources and health risks, *J. Hazard. Mater. Adv.,* **16,** 100 459.

Saneiyan, S., Filippone, N., Colwell, F. & Ntarlagiannis, D., 2024. Tracking microbial movement in saturated media with spectral induced polarization, *J. Environ. Manage.,* **370,** 122 808.

Schweitzer, P.A., 2004. *Corrosion Resistance Tables: Metals, Non-metals, Coatings, Mortars, Plastics, Elastomers and Linings, and Fabrics*. CRC Press.

Sivan, A., Szanto, M. & Pavlov, V., 2006. Biofilm development of the polyethylene-degrading bacterium rhodococcus ruber, *Appl. Microbiol. Biotechnol.,* **72,** 346–352.

Slater, L.D. & Lesmes, D., 2002. IP interpretation in environmental investigations, *Geophysics,* **67,** 77–88.

Song, Y. *et al.* 2024. Spectral induced polarization response of bacteria growth and decay in soil column experiments, *J. Geophys. Res. Biogeosciences,* **129,** e2024JG008050.

Song, Y., Shi, X., Revil, A. & Kang, X., 2022. Monitoring in situ microbial growth and decay in soil column experiments by induced polarization, *Geophys. Res. Lett.,* **49,** e2021GL097553.

Tindall, B.J., Rosselló-Móra, R., Busse, H.-J., Ludwig, W. & Kämpfer, P., 2010. Notes on the characterization of prokaryote strains for taxonomic purposes, *Int. J. Syst. Evol. Microbiol.,* **60,** 249–266.

Truskewycz, A., Gundry, T.D., Khudur, L.S., Kolobaric, A., Taha, M., Aburto-Medina, A., Ball, A.S. & Shahsavari, E., 2019. Petroleum hydrocarbon contamination in terrestrial ecosystems-fate and microbial responses, *Mol. Basel Switz.,* **24,** 3400.

Vecht, S.E., Platt, M.W., Er-El, Z. & Goldberg, I., 1988. The growth of *Pseudomonas putida* on m-toluic acid and on toluene in batch and in chemostat cultures, *Appl. Microbiol. Biotechnol.,* **27,** 587–592.

Vilas-Boas, A.C.M., Tarelho, L.A.C., Moura, J., Gomes, H., Marques, C., Pio, D.T., Nunes, M.I. & Silvestre, A.J.D., 2024. Methodologies for bio-oil characterization from biomass pyrolysis: a review focused on GC-MS, *J. Anal. Appl. Pyrolysis,* **185,** 1–20.

Vinegar, H.J. & Waxman, M.H., 1984. Induced polarization of shaly sands, *Geophysics,* **49,** 1267–1287.

Wal, A.v.d., Norde, W., Zehnder, A.J.B. & Lyklema, J., 1997. Determination of the total charge in the cell walls of gram-positive bacteria, *Colloids Surf. B Biointerfaces,* **9,** 81–100.

Warhurst, A.M. & Fewson, C.A., 1994. Biotransformations catalyzed by the genus *Rhodococcus*, *Crit. Rev. Biotechnol.,* **14,** 29–73.

Wheeler, J.D., Secchi, E., Rusconi, R. & Stocker, R., 2019. Not just going with the flow: the effects of fluid flow on bacteria and plankton, *Annu. Rev. Cell Dev. Biol.,* **35,** 213–237.

Zhang, C., Revil, A., Fujita, Y., Munakata-Marr, J. & Redden, G., 2014. Quadrature conductivity: a quantitative indicator of bacterial abundance in porous media, *Geophysics,* **79,** D363–D375.

Zhang, Z. & Furman, A., 2023. Statistical analysis for biogeochemical processes in a sandy column with dynamic hydrologic regimes using spectral induced polarization (SIP) and self-potential (SP), *Geophys. J. Int.,* **233,** 564–585.

Zwietering, M.H., Jongenburger, I., Rombouts, F.M. & Riet, K.v.'t., 1990. Modeling of the bacterial growth curve, *Appl. Environ. Microbiol.,* **56,** 1875–1881.